https://doi.org/10.15407/ujpe70.10.727

A.V. KOROTUN [1, 2]

[1] National University "Zaporizhzhia Polytechnic"
(64, Zhukovs'kogo Str., Zaporizhzhya 69011, Ukraine)
[2] G.V. Kurdyumov Institute for Metal Physics, Nat. Acad. of Sci. of Ukraine
(36, Akademika Vernads'kogo Blvd., Kyiv 03142, Ukraine; e-mail: andko@zp.edu.ua)

RESONANT OPTICAL PHENOMENA IN METALLIC DUMBBELL-SHAPED NANOPARTICLES. EQUIVALENT-SPHEROID APPROACH

Expressions for the diagonal components of the Q-factor, local electric field enhancement, and polarizability tensors, as well as the absorption, scattering, and extinction cross-sections have been obtained for metallic dumbbell-shaped nanoparticles in the classical approximation. The equivalent-spheroid approach is used to develop an analytic theory. The calculation results for the indicated optical characteristics are obtained for dumbbell-shaped nanoparticles of various sizes and materials. The influence of the particle's effective aspect ratio on the frequency dependences of the studied optical characteristics has been analyzed. The feasibility of using dumbbell-shaped nanoparticles with small aspect ratios in nanomedicine and as optical high-Q resonators has been shown.

Keywords: dumbbell-shaped nanoparticle, polarizability tensor, field enhancement, *Q*-factor, absorption, scattering cross-section, extinction cross-section, equivalent-spheroid approach, effective aspect ratio, surface plasmon resonance.

1. Introduction

Metallic nanoparticles, especially those made of noble metals, are important due to their extraordinary efficiency as light absorbers and scatterers. These phenomena are explained as a result of collective oscillations of conduction electrons excited near the metal surface by light with a certain frequency [1]. The optical properties of metallic nanoparticles, in particular axisymmetric ones, find applications in micro- and optoelectronics [2,3], biomedical imaging [2,4–6], surface plasmon resonance sensors [7, 8], and catalysis.

It is known that the size and shape of nanostructures significantly affect their optical properties [9–11]. In particular, in works [12–21] it was found that the nanoparticle shape substantially influences the frequency dependences of the absorption and scattering cross-sections of light by non-spherical metallic nanoparticles, and such characteristics as optical conductivity, polarizability, and relaxation rate are diagonal tensors of the second rank. Due to the morphological dependence of the optical properties of nanoparticles, the control over their shape and size is the focus of many studies. Various methods are used to obtain axisymmetric metallic nanoparticles, including electrochemical deposition on solid templates [22], electrochemical synthesis in solutions [9, 23], photochemical synthesis [23], and wet chemical synthesis [24].

The interest in the practical use of rod-shaped nanostructures of plasmonic metals is based on the fact that their optoelectronic properties can be comtrolled within a wide range – from the visible region to the near infrared one – by varying the aspect ratio of the particles [17–21], their crystallinity, and their environment in the colloidal solution. For example, a modification of the end part of nanorods can lead to a shift of the longitudinal surface plasmon resonance by up to 100 nm [25]. In addition, chemicals adsorbed on the nanorod surface exhibit surface-enhanced Raman scattering (SERS) owing to the interaction of surface plasmons with the molecular electronic states via photoexcitation [24, 26]. Axisymmetric particles of noble metals, which are shaped like dumbbells,

Citation: Korotun A.V. Resonant optical phenomena in metallic dumbbell-shaped nanoparticles. Equivalent-spheroid approach. *Ukr. J. Phys.* **70**, No. 10, 727 (2025). https://doi.org/10.15407/ujpe70.10.727.

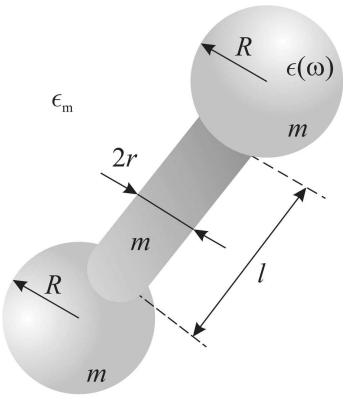

Fig. 1. Geometry of the problem

bones, and "phi" figure, constitute an important class of nanostructures, because they are candidates for application in nanomedicine; in particular, for the photothermal therapy of malignant neoplasms [27].

Dumbbell-shaped nanoparticles of plasmonic metals can be synthesized making use of several methods [25, 28–30]. Some of them are almost identical to the methods for synthesizing nanorods. As a result, the final size and shape of the particles depend on the time intervals of the key synthesis steps [25, 30]. The structure of axisymmetric particles was studied in works [31, 32]. Interestingly, the side faces were found to differ from the faces near the nanorod tips: the latter have a higher refractive index (i.e., they have a higher energy and form a more open structure) than the former [25, 30–32]. Regions with a higher refractive index can grow faster than the nanorod side surfaces so that dumbbell-shaped particles can be formed with a high probability under proper synthesis conditions. In those works, it was also shown that the overall appearance of the spectral profiles of colloidal dumbbell-shaped particles is quite similar to that of colloidal nanorods; however, the formation of spherical ends induces a red shift of the transverse and longitudinal localized surface plasmon resonances [25].

In works [33–35], optical effects in gold dumbbell-shaped nanoparticles coated with silver were studied, and it was shown that gold dumbbells can assemble into multi-particle structures due to steric hindrance effects. In the cited works, it was also found that dumbbell-shaped nanoparticles tend to couple with one another, in contrast to their arrangement in nanorods. Such configurations of dumbbell-shaped nanoparticles should demonstrate interesting optical properties, such as the mode hybridization and the emergence of hot spots and high-mobility plasmon peaks.

However, before studying the optical properties of assemblies of dumbbell-shaped nanoparticles, it is necessary to analyze the properties of individual particles. Therefore, the study of the optical properties of single dumbbell-shaped nanoparticles is a challenging task.

2. Basic Relationships

2.1. Formulation of the problem

Let a metallic nanoscale dumbbell-shaped particle be located in a dielectric medium with the permeability $\epsilon_{\rm m}$ (Fig. 1). The optical properties of such a nanoparticle can be described using the equivalent-spheroid approach [18, 19, 21, 36]; for the objects under study, a prolate spheroid is relevant. Therefore, the relationship for the diagonal components of the polarizability tensor has the same form as for a spheroidal nanoparticle,

$$\alpha_{\perp(\|)}\left(\omega\right) = V\frac{\epsilon^{\perp(\|)}\left(\omega\right)-\epsilon_{\rm m}}{\epsilon_{\rm m}+\mathcal{L}_{\perp(\|)}\left[\epsilon^{\perp(\|)}\left(\omega\right)-\epsilon_{\rm m}\right]}, \tag{1}$$

where V is the particle volume, $\mathcal{L}_{\perp(\|)}$ are the spheroid depolarization factors, and the diagonal components of the permittivity tensor of the nanoparticle material are

$$\epsilon^{\perp(\|)}\left(\omega\right) = \epsilon^{\infty} - \frac{\omega_p^2}{\omega\left(\omega+{\rm i}\gamma_{\rm eff}^{\perp(\|)}\right)}. \tag{2}$$

Here, ϵ^{∞} is the summand describing the contribution of the ionic core, $\omega_p = \sqrt{e^2 n_e/\left(\epsilon_0 m^*\right)}$ is the plasma frequency, n_e is the concentration of conduction electrons, m^* is the effective electron mass, ϵ_0 is the electric constant, and diagonal components of the effective relaxation rate tensor are

$$\gamma_{\rm eff}^{\perp(\|)} = \gamma_{\rm bulk} + \gamma_{\rm s}^{\perp(\|)} + \gamma_{\rm rad}^{\perp(\|)}, \tag{3}$$

where $\gamma_{\rm bulk} = {\rm const}$ is the bulk relaxation rate, and the diagonal components of the surface relaxation, $\gamma_{\rm s}$, and radiative damping, $\gamma_{\rm rad}$, rate tensors are

$$\gamma_{\rm s}^{\perp} = \frac{9}{16}\frac{\mathcal{L}_{\perp}}{\epsilon_{\rm m}+\mathcal{L}_{\perp}\left(1-\epsilon_{\rm m}\right)}\left(\frac{\omega_p}{\omega}\right)^2\frac{v_{\rm F}}{\ell_{\perp}}\mathcal{F}_{\perp}\left(\varrho_{\rm eff}\right), \tag{4}$$

$$\gamma_{\rm s}^{\|} = \frac{9}{16}\frac{\mathcal{L}_{\|}}{\epsilon_{\rm m}+\mathcal{L}_{\|}\left(1-\epsilon_{\rm m}\right)}\left(\frac{\omega_p}{\omega}\right)^2\frac{v_{\rm F}}{\ell_{\|}}\mathcal{F}_{\|}\left(\varrho_{\rm eff}\right), \tag{5}$$

$$\gamma_{\rm rad}^{\perp} = \frac{9V}{256\pi} \frac{\mathcal{L}_{\perp}}{\sqrt{\epsilon_{\rm m}\left[\epsilon^{\infty} + \left(\frac{1}{\mathcal{L}_{\perp}} - 1\right)\epsilon_{\rm m}\right]}} \times$$

$$\times \left(\frac{\omega_p}{c}\right)^3 \left(\frac{\omega_p}{\omega}\right)^2 \frac{v_{\rm F}}{\ell_{\perp}} \mathcal{F}_{\perp}\left(\varrho_{\rm eff}\right), \tag{6}$$

$$\gamma_{\rm rad}^{\parallel} = \frac{9V}{128\pi} \frac{\mathcal{L}_{\parallel}}{\sqrt{\epsilon_{\rm m}\left[\epsilon^{\infty} + \left(\frac{1}{\mathcal{L}_{\parallel}} - 1\right)\epsilon_{\rm m}\right]}} \times$$

$$\times \left(\frac{\omega_p}{c}\right)^3 \left(\frac{\omega_p}{\omega}\right)^2 \frac{v_{\rm F}}{\ell_{\parallel}} \mathcal{F}_{\parallel}\left(\varrho_{\rm eff}\right). \tag{7}$$

In formulas (4)–(7), c is the speed of light, $v_{\rm F}$ is the Fermi velocity of electrons, $\ell_{\perp(\parallel)}$ are the effective lengths of the transverse ($\perp$) and longitudinal ($\parallel$) fre e paths of electrons, and $\mathcal{F}_{\perp(\parallel)}\left(\varrho_{\rm eff}\right)$ are the following size-dependent functions for a prolate spheroid [18]:

$$\mathcal{F}_{\perp}\left(\varrho_{\rm eff}\right) = \left(1 - \varrho_{\rm eff}^2\right)^{-3/2} \times$$

$$\times \left\{2\left(\frac{3}{4} - \varrho_{\rm eff}^2\right)\left(\frac{\pi}{2} - \arcsin\varrho_{\rm eff}\right) + \right.$$

$$\left. + \varrho_{\rm eff}\left(3/2 - \varrho_{\rm eff}^2\right)\sqrt{1 - \varrho_{\rm eff}^2}\right\}, \tag{8}$$

$$\mathcal{F}_{\parallel}\left(\varrho_{\rm eff}\right) = \left(1 - \varrho_{\rm eff}^2\right)^{-3/2} \times$$

$$\times \left\{\frac{\pi}{2} - \arcsin\varrho_{\rm eff} + \varrho_{\rm eff}\left(1 - 2\varrho_{\rm eff}^2\right)\sqrt{1 - \varrho_{\rm eff}^2}\right\}, \tag{9}$$

where $\varrho_{\rm eff}$ is the effective aspect ratio; its relationship with the sizes of dumbbell-shaped nanoparticle will be obtained below.

The dependences of the depolarization factors on the effective aspect ratio are as follows [18, 19]:

$$\mathcal{L}_{\parallel} = \frac{\varrho_{\rm eff}^2}{2\left(1 - \varrho_{\rm eff}^2\right)^{3/2}} \times$$

$$\times \left(\ln\frac{1 + \sqrt{1 - \varrho_{\rm eff}^2}}{1 - \sqrt{1 - \varrho_{\rm eff}^2}} - 2\sqrt{1 - \varrho_{\rm eff}^2}\right), \tag{10}$$

$$\mathcal{L}_{\perp} = \frac{1}{2} - \frac{\varrho_{\rm eff}^2}{4\left(1 - \varrho_{\rm eff}^2\right)^{3/2}} \times$$

$$\times \left(\ln\frac{1 + \sqrt{1 - \varrho_{\rm eff}^2}}{1 - \sqrt{1 - \varrho_{\rm eff}^2}} - 2\sqrt{1 - \varrho_{\rm eff}^2}\right). \tag{11}$$

2.2. Effective aspect ratio

Before proceeding to derive the expressions for the effective aspect ratio and the effective electron mean free paths, let us make an important remark. Unlike other axisymmetric nanoparticles (cylinders, spherocylinders, disks), dumbbell-shaped particles are characterized by three geometric parameters: the radius R of the spherical part, as well as the length l and the base radius r of the cylindrical part. In addition, the masses of the parts of the dumbbell-shaped nanoparticle can be different. All those circumstances make it impossible to directly apply the equivalent-spheroid approach.

Therefore, let us consider such dumbbell-shaped nanoparticles, where the masses of the spherical and cylindrical parts are identical. Consequently, the volumes of the indicated parts are also the same. Whence the radius of the spherical part of a dumbbell-shaped nanoparticle is

$$R = \sqrt[3]{\frac{3}{4}r^2 l}. \tag{12}$$

According to the ideology of the equivalent-spheroid approach, the effective aspect ratio is determined from the equality condition for the ratios between the axial moments of inertia of a dumbbell-shaped particle and a prolate spheroid. Therefore, let us find the corresponding moments of inertia for the dumbbell-shaped (db) nanoparticle with respect to the axis coinciding with the axis of the cylindrical part and the axis perpendicular to it and passing through the center of mass of the particle,

$$I_z^{\rm db} = m\left(\frac{r^2}{2} + \frac{4}{5}R^2\right), \tag{13}$$

$$I_x^{\rm db} = m\left[\frac{3r^2 + l^2}{12} + 2\left(\frac{2}{5}R^2 + \left(\frac{l}{2} + R\right)^2\right)\right]. \tag{14}$$

For an equivalent prolate spheroid (ps), the corresponding quantities look like

$$I_z^{\rm ps} = \frac{2}{5}mb^2, \tag{15}$$

$$I_x^{\rm ps} = \frac{1}{5}m\left(a^2 + b^2\right). \tag{16}$$

Hence, the ratio between the axial moments of inertia is as follows:

• for an equivalent prolate spheroid,

$$\frac{I_x^{\rm ps}}{I_z^{\rm ps}} = \frac{1}{2\varrho_{\rm eff}^2} + \frac{1}{2}, \tag{17}$$

where $\varrho_{\rm eff} = b/a$ is the effective aspect ratio;

• for a dumbbell-shaped nanoparticle with regard for Eq. (12)],

$$\frac{I_x^{\rm ds}}{I_z^{\rm ds}} = {\rm H}\,(\varrho), \tag{18}$$

where

$$\begin{aligned}{\rm H}\,(\varrho) = \\ = \frac{\frac{1}{12}\left(3\varrho^2+1\right) + 2\left[\frac{2}{5}\left(\frac{3}{4}\varrho^2\right)^{\frac{2}{3}} + \left(1+\left(\frac{3}{4}\varrho^2\right)^{\frac{1}{3}}\right)^2\right]}{\frac{\varrho^2}{2} + \frac{4}{5}\left(\frac{3}{4}\varrho^2\right)^{\frac{2}{3}}},\end{aligned} \tag{19}$$

and $\varrho = r/l$.

Equating expressions (17) and (18), we obtain

$$\varrho_{\rm eff} = \frac{1}{\sqrt{2{\rm H}\,(\varrho) - 1}}. \tag{20}$$

2.3. Effective electron mean free paths

The transverse ($\perp$) and longitudinal ($\|$) effective electron mean free paths are as follows:

• for a prolate spheroid,

$$\ell_\| = 2a, \quad \ell_\perp = 2b; \tag{21}$$

• for a dumbbell-shaped nanoparticle,

$$\begin{aligned}&\ell_\| = l + 4R,\\ &\ell_\perp = \begin{cases} 2R,\ \ell_\| \in (0,\ 2R) \cup (2R+l,\ 4R+l);\\ 2r,\ \ell_\| \in (2R,\ l+2R),\end{cases}\end{aligned}$$

or taking relationship (12) into account,

$$\begin{aligned}&\ell_\| = l + 4\sqrt[3]{\frac{3}{4}r^2 l},\\ &\ell_\perp = \begin{cases} 2\sqrt[3]{\frac{3}{4}r^2 l},\ \ell_\| \in \left(0,\ 2\sqrt[3]{\frac{3}{4}r^2 l}\right) \cup\\ \cup \left(2\sqrt[3]{\frac{3}{4}r^2 l} + l,\ 4\sqrt[3]{\frac{3}{4}r^2 l} + l\right);\\ 2r,\ \ell_\| \in \left(2\sqrt[3]{\frac{3}{4}r^2 l},\ l + 2\sqrt[3]{\frac{3}{4}r^2 l}\right).\end{cases}\end{aligned} \tag{22}$$

2.4. Extinction cross-section, Q-factor tensors, and field enhancement

As is known, the measured optical characteristic of metallic nanoparticles of various shapes is the extinction cross-section [37]

$$C_{\rm ext} = C_{\rm abs} + C_{\rm sca}, \tag{23}$$

where the absorption cross-section $C_{\rm abs}$ and the scattering cross-section $C_{\rm sca}$ are determined by the formulas

$$C_{\rm abs} = \frac{\omega\sqrt{\epsilon_{\rm m}}}{c}{\rm Im}\left(\frac{2}{3}\alpha_\perp + \frac{1}{3}\alpha_\|\right), \tag{24}$$

$$C_{\rm sca} = \frac{\omega^4\epsilon_{\rm m}^2}{6\pi c^4}\left(\frac{2}{3}|\alpha_\perp|^2 + \frac{1}{3}|\alpha_\|\,|^2\right). \tag{25}$$

Important for practical applications of metallic nanoparticles are such optical characteristics as the field enhancement $\mathcal{G}$ and the Q-factor. Due to the absence of spherical symmetry and the presence of axial symmetry in dumbbell-shaped particles, the indicated characteristics are diagonal tensors of the second rank,

$$\mathcal{G} = \begin{pmatrix} \mathcal{G}_\perp & 0 & 0\\ 0 & \mathcal{G}_\perp & 0\\ 0 & 0 & \mathcal{G}_\| \end{pmatrix}, \quad Q = \begin{pmatrix} Q_\perp & 0 & 0\\ 0 & Q_\perp & 0\\ 0 & 0 & Q_\| \end{pmatrix}. \tag{26}$$

It is well known that effects associated with the direction along the larger nanoparticle size (for example, the widespread use of the longitudinal surface plasmon resonance in axisymmetric nanoparticles of various shapes) are of dominant (prevailing) importance. Therefore, it is interesting, first of all, to study the frequency dependences of the longitudinal components of the field enhancement and Q-factor tensors. So, let us write down the relationships for those components,

$$\mathcal{G}_\| = \left|\frac{\epsilon^\|\,(\omega)}{\mathcal{L}_\|\epsilon^\|\,(\omega) + \left(1-\mathcal{L}_\|\right)\epsilon_{\rm m}}\right|^2, \tag{27}$$

$$Q_\| = \frac{\omega}{2\,{\rm Im}\epsilon^\|(\omega)}\frac{d}{d\omega}\left[{\rm Re}\,\epsilon^\|(\omega)\right]. \tag{28}$$

Using expression (2), formula (28) can be rewritten in the form

$$Q_\| = \frac{\omega_p^2}{\gamma_{\rm eff}^\|\left(\omega^2 + \gamma_{\rm eff}^{\|\,2}\right)}\left[\omega + \gamma_{\rm eff}^\|\frac{d\gamma_{\rm eff}^\|}{d\omega}\right], \tag{29}$$

where

$$\frac{d\gamma_{\text{eff}}^{\parallel}}{d\omega} = -\frac{2\mathcal{K}_{\parallel}}{\omega^3} \tag{30}$$

and

$$\mathcal{K}_{\parallel} = \frac{9}{32}\mathcal{L}_{\parallel}\omega_p^2\frac{v_{\text{F}}}{\ell_{\parallel}}\mathcal{F}_{\parallel}\left(\varrho_{\text{eff}}\right)\times$$

$$\times\left\{\frac{1}{\epsilon_{\text{m}}+\mathcal{L}_{\parallel}(1-\epsilon_{\text{m}})}+\frac{V\left(\frac{\omega_p}{c}\right)^3}{4\sqrt{\epsilon_{\text{m}}\left[\epsilon^{\infty}+\left(\frac{1}{\mathcal{L}_{\parallel}}-1\right)\epsilon_{\text{m}}\right]}}\right\}. \tag{31}$$

In what follows, we will use relationships (1), (23), (27), and (29) in view of expressions (2)–(11), (20)–(22), (24), (25), (30), and (31).

3. Calculation Results and Their Discussion

The calculations are performed for dumbbell-shaped nanoparticles made of various metals and having various sizes, which were located in Teflon ($\epsilon_{\text{m}} = 2.3$). The metal parameters required for calculations are quoted in Table 1.

In Figs. 2 and 3, the frequency dependences of the real and imaginary parts, as well as the absolute values, of the diagonal components of the polarizability tensor of dumbbell-shaped Ag particles are plotted. As in the case of nanoparticles with other shapes, the functions $\operatorname{Re}\alpha_{\perp(\parallel)}(\omega)$ are sign-changing (Figs. 2, *a* and 3, *a*), whereas $\operatorname{Im}\alpha_{\perp(\parallel)}(\omega)$ are always positive (Figs. 2, *b* and 3, *b*). Note that since $\operatorname{Re}\alpha_{\perp(\parallel)} \sim \operatorname{Im}\alpha_{\perp(\parallel)}$, the both components make approximately identical contributions to $\left|\alpha_{\perp(\parallel)}\right|$ (Figs. 2, *c* and 3, *c*). In addition, the calculations showed that $\operatorname{Re}\alpha_{\parallel} \gg \operatorname{Re}\alpha_{\perp}$, $\operatorname{Im}\alpha_{\parallel} \gg \operatorname{Im}\alpha_{\perp}$, so, accordingly, $\left|\alpha_{\parallel}\right| \gg |\alpha_{\perp}|$. In this regard, the main contribution to the absorption, scattering, and extinction cross-sections is given by the real and imaginary parts, and the absolute value of the longitudinal polarization component. Note that the maxima of the imaginary parts, which correspond to the longitudinal and transverse surface plasmon resonances, are located in different spectral intervals. In particular, the frequencies of transverse resonances are in the near-ultraviolet part of the spectrum, while the frequencies

Table 1. **Parameters of metals (see, e.g., works [19, 21])**

Metal	Parameter				
	z	r_s/a_0	m^*/m_e	ϵ^{∞}	γ_{bulk}, 10^{13} s^{-1}
Pd	2	4.00	0.37	2.52	13.9
Pt	2	3.27	0.54	4.42	10.52
Ag	1	3.02	0.96	3.70	2.50
Au	1	3.01	0.99	9.84	3.45
Cu	1	2.11	1.49	12.03	3.70

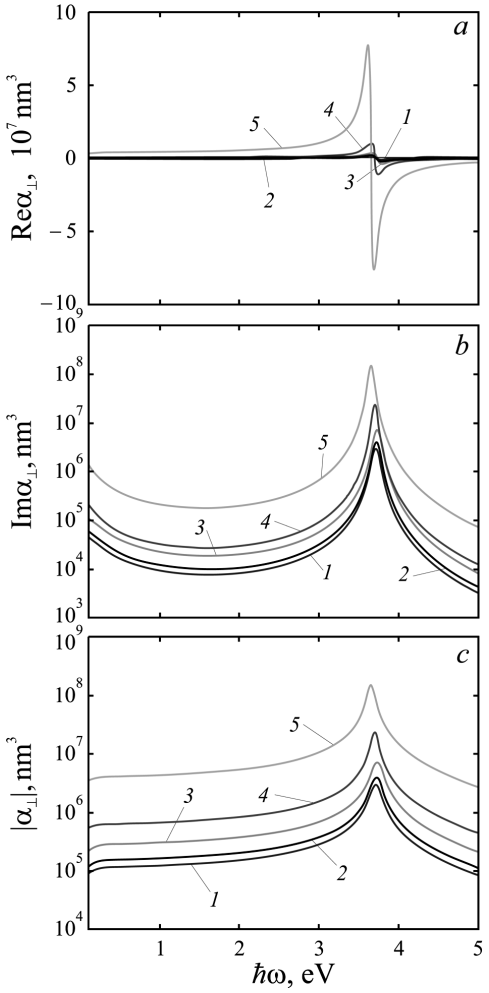

Fig. 2. Frequency dependences of the real (*a*) and imaginary (*b*) parts, as well as the absolute value (*c*) of the transverse component of the polarization tensor of a dumbbell-shaped Ag nanoparticle in Teflon for various particle sizes: $r = 10$ nm, $l = 60$ nm (*1*); $r = 10$ nm, $l = 80$ nm (*2*); $r = 10$ nm, $l = 150$ nm; (*3*) $r = 20$ nm, $l = 80$ nm (*4*); $r = 50$ nm, $l = 80$ nm (*5*)

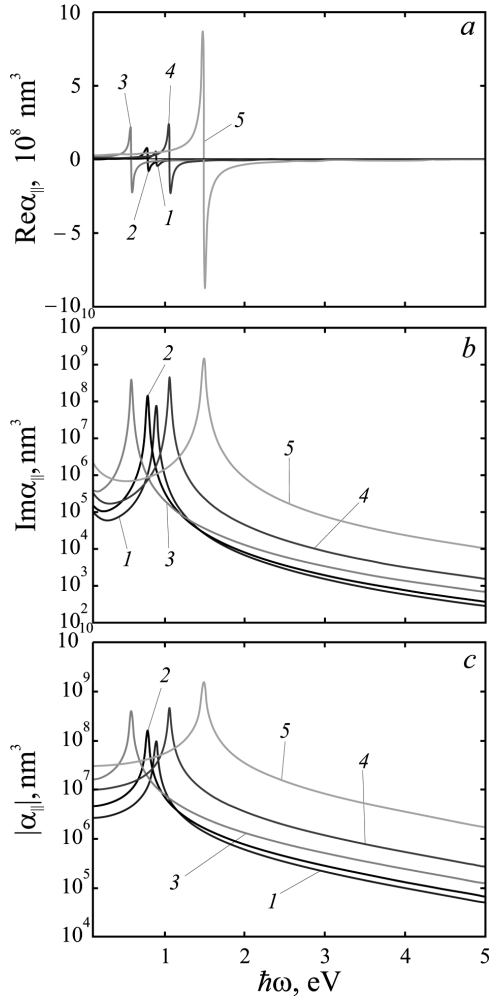

Fig. 3. Frequency dependences of the real (*a*) and imaginary (*b*) parts, as well as the absolute value (*c*) of the longitudinal component of the polarization tensor of a dumbbell-shaped Ag nanoparticle in Teflon for various particle sizes: $r = 10$ nm, $l = 60$ nm (*1*); $r = 10$ nm, $l = 80$ nm (*2*); $r = 10$ nm, $l = 150$ nm (*3*); $r = 20$ nm, $l = 80$ nm (*4*); $r = 50$ nm, $l = 80$ nm (*5*)

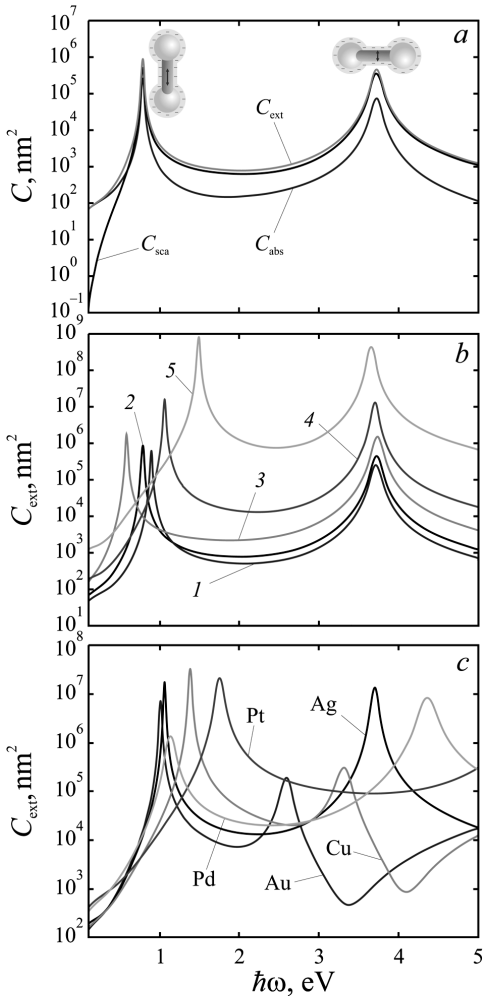

Fig. 4. Frequency dependences of absorption, scattering, and extinction cross-sections for dumbbell-shaped metal nanoparticles in Teflon: comparison of their contributions (Ag particles with $r = 10$ nm and $l = 80$ nm) (*a*); extinction cross-sections for various sizes of dumbbell-shaped Ag nanoparticles (*b*): $r = 10$ nm, $l = 60$ nm (*1*); $r = 10$ nm, $l = 80$ nm (*2*); $r = 10$ nm, $l = 150$ nm (*3*); $r = 20$ nm, $l = 80$ nm (*4*); $r = 50$ nm, $l = 80$ nm (*5*); extinction cross-sections of dumbbell-shaped nanoparticles ($r = 10$ nm, $l = 80$ nm) of various metals (*c*)

of longitudinal resonances are in the visible (optical) and near-infrared regions (Figs. 2, *b* and 3, *b*). As concerning the shifts of $\max\{\mathrm{Im}\,\alpha_{\perp(\parallel)}\}$, when changing the aspect ratio (the variation of the nanoparticle length and the cross-section radius of the cylindrical particle), we note that the growth of the aspect ratio along the curve sequences $3 \to 2 \to 1$ and $2 \to 4 \to 5$ results in a slight "red" shift of $\max\{\mathrm{Im}\,\alpha_{\perp}\}$ and a more substantial "blue" shift of $\max\{\mathrm{Im}\,\alpha_{\parallel}\}$, i.e., in the "attraction" of those maxima.

The frequency dependences of the absorption, scattering, and extinction cross-sections are shown in Fig. 4. The calculation results demonstrate that, unlike nanoparticles with other geometries, the scattering cross-section for dumbbell-shaped nanoparticles is an order of magnitude larger than the absorption cross-section in the optical spectral interval. The-

refore, the scattering losses are also an order of magnitude higher than the heating losses (Fig. 4, *a*). In turn, an increase in the effective aspect ratio results in a decrease of the distance between the extinction cross-section maxima (the "attraction" of the maxima); see Fig. 4, *b*. Since those maxima correspond to the frequences of the transverse and longitudinal surface plasmon resonances, then the difference between the resonance frequences decreases as the effective aspect ratio increases. This fact is confirmed by numerical calculations of the resonance frequences $\omega_{sp}^{\perp(\parallel)}$ for various metals and various ϱ_{eff} values (Table 2).

Table 2. **Frequences of transverse, $\omega_{sp}^{\perp}$, and longitudinal, $\omega_{sp}^{\parallel}$, surface plasmon resonances and their splitting $\Delta\omega_{sp}$ for dumbbell-shaped nanoparticles of various metals in Teflon at various aspect ratio values**

Metal	ϱ_{eff}	$\omega_{sp}^{\perp}$, eV	$\omega_{sp}^{\parallel}$, eV	$\Delta\omega_{sp}$, eV
Au	0.1	2.593	0.825	1.769
	0.2	2.575	1.299	1.276
	0.3	2.553	1.612	0.941
	0.4	2.529	1.830	0.699
	0.5	2.505	1.989	0.516
	0.6	2.481	2.109	0.372
	0.7	2.457	2.202	0.255
	0.8	2.433	2.277	0.157
	0.9	2.410	2.337	0.073
Ag	0.1	3.712	0.855	2.857
	0.2	3.660	1.404	2.256
	0.3	3.599	1.814	1.758
	0.4	3.536	2.136	1.400
	0.5	3.473	2.394	1.078
	0.6	3.410	2.608	0.803
	0.7	3.350	2.786	0.564
	0.8	3.292	2.938	0.354
	0.9	3.235	3.068	0.167
Cu	0.1	3.317	1.135	2.182
	0.2	3.297	1.765	1.532
	0.3	3.273	2.165	1.108
	0.4	3.247	2.436	0.812
	0.5	3.221	2.628	0.593
	0.6	3.194	2.770	0.424
	0.7	3.168	2.879	0.289
	0.8	3.141	2.640	0.177
	0.9	3.115	3.033	0.082
Pt	0.1	5.833	1.415	4.418
	0.2	5.759	2.313	3.446
	0.3	5.673	2.979	2.701
	0.4	5.583	3.480	2.013
	0.5	5.492	3.884	1.609
	0.6	5.403	4.211	1.192
	0.7	5.316	4.482	0.834
	0.8	5.231	4.709	0.521
	0.9	5.149	4.903	0.246

Table 3. **Calculated values of the transverse, $\gamma_{\text{eff}}^{\perp}$, and longitudinal, $\gamma_{\text{eff}}^{\parallel}$, effective relaxation rates for dumbbell-shaped nanoparticles of various metals in Teflon at various aspect ratio values**

Metal	ϱ_{eff}	$\gamma_{\text{eff}}^{\perp}$, eV	$\gamma_{\text{eff}}^{\parallel}$, eV
Au	0.1	1.315	0.030
	0.2	0.152	0.028
	0.3	0.103	0.030
	0.4	0.096	0.036
	0.5	0.114	0.052
	0.6	0.158	0.086
	0.7	0.233	0.150
	0.8	0.346	0.264
	0.9	0.507	0.452
Ag	0.1	0.679	0.024
	0.2	0.085	0.022
	0.3	0.062	0.023
	0.4	0.063	0.028
	0.5	0.081	0.042
	0.6	0.118	0.071
	0.7	0.179	0.124
	0.8	0.270	0.216
	0.9	0.401	0.367
Cu	0.1	1.476	0.032
	0.2	0.178	0.031
	0.3	0.138	0.036
	0.4	0.159	0.054
	0.5	0.232	0.098
	0.6	0.364	0.190
	0.7	0.576	0.365
	0.8	0.889	0.675
	0.9	1.332	1.188
Pt	0.1	1.622	0.084
	0.2	0.258	0.085
	0.3	0.260	0.103
	0.4	0.369	0.162
	0.5	0.598	0.300
	0.6	0.992	0.583
	0.7	1.609	1.108
	0.8	2.523	2.016
	0.9	3.823	3.497

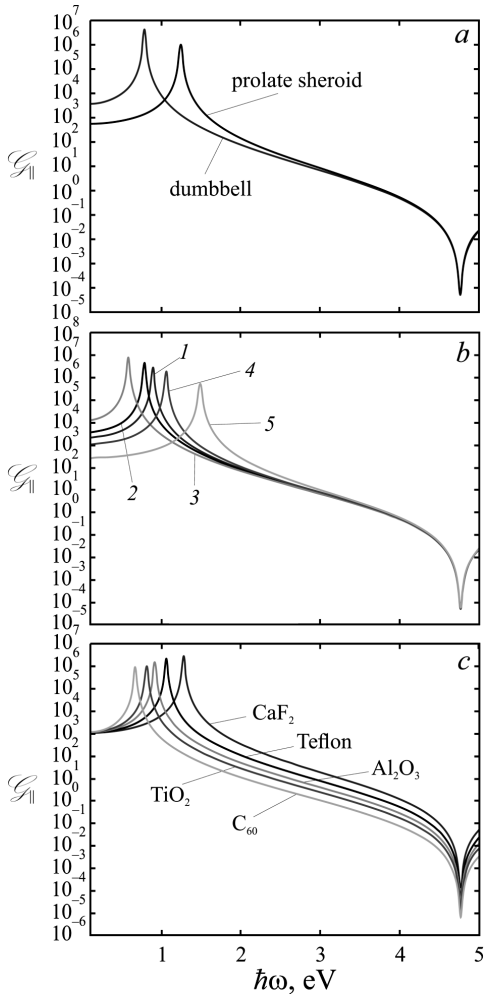

Fig. 5. Frequency dependences of the longitudinal component of the field enhancement tensor in the vicinity of prolate Ag nanoparticles: (*a*) comparison of the results obtained for dumbbell-shaped and spheroidal nanoparticles of the same volume in Teflon; (*b*) dumbbell-shaped nanoparticles of various sizes in Teflon: $r = 10$ nm, $l = 60$ nm (*1*); $r = 10$ nm, $l = 80$ nm (*2*); $r = 10$ nm, $l = 150$ nm (*3*); $r = 20$ nm, $l = 80$ nm (*4*); $r = 50$ nm, $l = 80$ nm (*5*); dumbbell-shaped nanoparticles ($r = 10$ nm, $l = 80$ nm) in various media (*c*)

Note the following circumstance concerning the widths of the resonance peaks of the extinction cross-section, which are determined by the corresponding effective relaxation rates. If the effective aspect ratio is small, then $\gamma_{\text{eff}}^{\perp} \gg \gamma_{\text{eff}}^{\parallel}$, $\gamma_{\text{eff}}^{\perp}$ and $\gamma_{\text{eff}}^{\parallel}$ increase as the effective aspect ratio increases, and the values of $\gamma_{\text{eff}}^{\parallel}$ approach $\gamma_{\text{eff}}^{\perp}$ (Table 3). This occurs due to the fact that if ϱ_{eff} is small, the ratio r/l is also small, and,

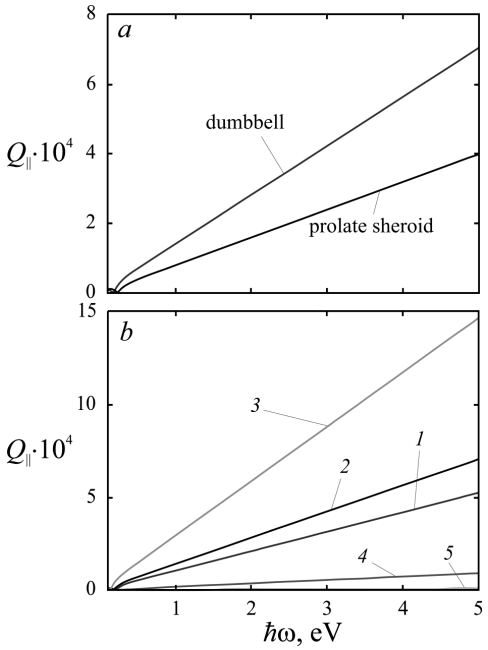

Fig. 6. Frequency dependences of the longitudinal component of the Q-factor tensor for prolate Ag nanoparticles: comparison of the results obtained for dumbbell-shaped and spheroidal nanoparticles of the same volume in Teflon (*a*); dumbbell-shaped nanoparticles of various sizes in Teflon (*b*): $r = 10$ nm, $l = 60$ nm (*1*); $r = 10$ nm, $l = 80$ nm (*2*); $r = 10$ nm, $l = 150$ nm (*3*); $r = 20$ nm, $l = 80$ nm (*4*); $r = 50$ nm, $l = 80$ nm (*5*)

consequently, electrons moving in the radial direction collide more often with the surface, and the transverse component of the surface relaxation rate tensor is large. Hence, the width of the maximum corresponding to the transverse surface plasmon resonance is also large. Furthermore, the indicated quantities have a minimum in the interval $0.1 < \varrho_{\text{eff}} < 0.2$. However, $\min\left\{\gamma_{\text{eff}}^{\parallel}\right\}$ is barely noticeable (being absent at all for Pt nanoparticles), but $\min\left\{\gamma_{\text{eff}}^{\perp}\right\}$ is deep.

The frequency dependences of the extinction cross-sections for dumbbell-shaped nanoparticles of the same size, but of different metals, are qualitatively similar (the corresponding curves have two maxima). The positions of the maxima (the frequences of the longitudinal and transverse surface plasmon resonances) and the distance between them are determined by the optical properties of a particular metal (Fig. 4, *c*).

In Fig. 5, the frequency dependences of the longitudinal component of the field enhancement ten-

sor are depicted. A comparison of the dependences for spheroidal and dumbbell-shaped particles of the same volume (Fig. 5, *a*) demonstrates a qualitative similarity of the obtained results, but quantitatively they differ considerably in the near-infrared spectral region (in particular, this concerns the spectral position of $\max\{G_{\parallel}\}$). Thus, the identification of the optical properties of dumbbell-shaped and spheroidal nanoparticles of the same volume is possible only in the frequency ls, where the optical characteristics have no maxima. Note that this is not a specific feature of dumbbell-shaped nanoparticles because it was found in work [18] that the position of the longitudinal surface plasmon resonance for cylinders, spherocylinders, and prolate spheroids with the same volume depends on the nanoparticle geometry. The behavior and sequence of the frequency dependence curves for the longitudinal component of the electric field enhancement tensor for dumbbell-shaped nanoparticles with different effective aspect ratios (Fig. 5, *b*) are the same as those of the frequency dependence curves for the imaginary part of the longitudinal component of the polarizability tensor, and the maximum enhancement values (corresponding to the frequencies of longitudinal surface plasmon resonances) are quite substantial ($10^6 \div 10^7$). In turn, in the case of a dumbbell-shaped Ag nanoparticle in various insulators, the "blue" shift of $\max\{G_{\parallel}\}$ takes place as the permeability of the surrounding medium increases along the series $CaF_2 \to$ Teflon $\to Al_2O_3 \to$ $\to TiO_2 \to C_{60}$ (Fig. 5, *c*).

The frequency dependences of the longitudinal component the Q-factor tensor are shown in Fig. 6. The calculation results demonstrate that the longitudinal component of the Q-factor tensor of the dumbbell-shaped nanoparticle is larger than that of the prolate spheroidal particle within the entire examined spectral interval so that dumbbell-shaped particles have more prospects for their application as optical resonators (Fig. 6, *a*). Among dumbbell-shaped nanoparticles with various effective aspect ratios, the longitudinal component of the Q-factor tensor is the largest for particles with the smallest effective aspect ratio (Fig. 6, *b*).

4. Conclusions

In the framework of the equivalent-spheroid approach, the relationships for the diagonal components of the polarization, field enhancement, and Q-factor tensors, as well as the absorption, scattering, and extinction cross-sections for metallic dumbbell-shaped nanoparticles have been obtained. It is shown that the maxima in the optical characteristics of dumbbell nanoparticles, which correspond to the longitudinal and transverse surface plasmon resonances, are strongly different by frequency, which greatly facilitates the use of longitudinal resonance, in particular, in nanomedicine, because this resonance falls into one of the biological transparency windows.

It has been demonstrated that a decrease in the effective aspect ratio of a dumbbell-shaped nanoparticle results in a "repulsion" of resonances. Therefore, for practical applications, in particular, in nanomedicine, it is advisable to use nanoparticles with small effective aspect ratios.

The calculation results testify that, unlike nanoparticles with other shapes, the scattering cross-section of dumbbell-shaped particles is an order of magnitude larger than their absorption cross-section, which points to the dominance of radiation processes in nanoparticles with the examined shape.

It has been shown that the resonance peaks corresponding to the longitudinal resonance are always narrower than the peaks corresponding to the transverse resonance, and the width difference of the spectral peak (the effective relaxation rates) increases as the aspect ratio decreases.

It has been proved that the identification of the optical properties of dumbbell-shaped and spheroidal particles of the same volume at frequencies close to the resonant one is impossible because of a substantial discrepancy among the values of the longitudinal component of the field enhancement tensor. The expediency of using dumbbell-shaped nanoparticles rather than spheroidal ones as optical resonators has been established, because the longitudinal component of the Q-factor for the former is greater than that for the latter within the whole studied frequency interval.

A considerable dependence of the positions of the maxima of the optical characteristics – first of all, the extinction cross-section and the longitudinal component of the field enhancement tensor – on the nanoparticle material and the surrounding environment has been demonstrated, which is associated with a substantial difference of their optical and electrophysical parameters.

1. T. Patil, R. Gambhir, A. Vibhute, A.P. Tiwari. Gold nanoparticles: synthesis methods, functionalization and biological applications. *J. Cluster Sci.* **34**, 705 (2023).
2. M.M. Ghobashy, S.A. Alkhursani, H.A. Alqahtani, T.K. El-damhougy, M. Madani. Gold nanoparticles in microelectronics advancements and biomedical applications. *Mater. Sci. Eng.* **301**, 117191 (2024).
3. M.A. Morsi, A.H. Oraby, A.G. Elshahawy, R.M. Abd El-Hady. Preparation, structural analysis, morphological investigation and electrical properties of gold nanoparticles filled polyvinyl alcohol/carboxymethyl cellulose blend. *J. Mater. Res. Technol.* **8**, 5996 (2019).
4. J. Milan, K. Niemczyk, M. Kus-Liśkiewicz. Treasure on the Earth–gold nanoparticles and their biomedical applications. *Materials* **15**, 3355 (2022).
5. X. Zhang. Gold nanoparticles: recent advances in the biomedical applications. *Cell Biochem. Biophys.* **72**, 771 (2015).
6. X. Li, Y. Zhang, G.K. Liu, Z. luo, L. Zhou, Y. Xue, M. Liu. Recent progress in the applications of gold-based nanoparticles towards tumor-targeted imaging and therapy. *RSC Adv.* **12**, 7635 (2022).
7. J. Sun, Y. Lu, L. He, J. Pang, F. Yang, Y. Liu. Colorimetric sensor array based on gold nanoparticles: design principles and recent advances. *Trends Anal. Chem.* **122**, 115754 (2020).
8. G. Liu, M. Lu, X. Huang, T. Li, D. Xu. Application of gold-nanoparticle colorimetric sensing to rapid food safety screening. *Sensors* **18**, 4166 (2018).
9. Y.-Y. Yu, S.-S. Chang, C.-L. Lee, C.R.C. Wang. Gold nanorods: electrochemical synthesis and optical properties. *J. Phys. Chem. B* **101**, 6661 (1997).
10. M.-C. Daniel, D. Astruc. Gold nanoparticles: assembly, supramolecular chemistry, quantum-size-related properties, and applications toward biology, catalysis, and nanotechnology. *Chem. Rev.* **104**, 293 (2004).
11. B. Nikoobakht, M.A. El-Sayed. Surface-enhanced Raman scattering studies on aggregated gold nanorods. *J. Phys. Chem. A* **107**, 3372 (2003).
12. P.M. Tomchuk, N.I. Grigorchuk. Shape and size effects on the energy absorption by small metallic particles. *Phys. Rev. B* **73**, 155423 (2006).
13. N.I. Grigorchuk, P.M. Tomchuk. Force of optical radiation pressure on a spheroidal metallic nanoparticle near a plasmon resonance. *Low Temp. Phys.* **33**, 851 (2007).
14. N.I. Grigorchuk, P.M. Tomchuk. Optical and transport properties of spheroidal metal nanoparticles with account for the surface effect. *Phys. Rev. B* **84**, 085448 (2011).
15. N.I. Grigorchuk. Plasmon resonant light scattering on spheroidal metallic nanoparticle embedded in a dielectric matrix. *Europhys. Lett.* **97**, 45001 (2012).
16. P.M. Tomchuk. Dependence of the light scattering cross-section by metal nanoparticles on their shape. *Ukr. J. Phys.* **57**, 553 (2012).
17. A.V. Korotun, N.I. Pavlishche. Anisotropy of the optical properties of metal nanodisks. *Opt. Spectrosc.* **130**, 269 (2022).
18. A.V. Korotun, Ya.V. Karandas, V.I. Reva. Analytic theory of plasmon effects in rod-like metal nanoparticles. The equivalent-spheroid model. *Ukr. J. Phys.* **67**, 848 (2022).
19. A.V. Korotun. Plasmonic phenomena in biconical and bipyramidal metal nanoparticles. *Ukr. J. Phys.* **68**, 697 (2023).
20. A.V. Korotun. More on the size effects on the spectral figure of merit and enhancement of the local fields in the neighborhood of biconical and bipyramidal metallic nanoparticles. *Low Temp. Phys.* **51**, 133 (2025).
21. N.I. Pavlyshche, A.V. Korotun, V.P. Kurbatsky, V.I. Reva. Plasmon phenomena in metal-dielectric nanodiscs. An equivalent-spheroid approach. *Ukr. J. Phys.* **70**, 263 (2025).
22. C.A. Foss Jr., G.L. Hornyak, J.A. Stockert, C.R. Martin. Optical properties of composite membranes containing arrays of nanoscopic gold cylinders. *J. Phys. Chem.* **96**, 7497 (1992).
23. S.-S. Chang, C.-W. Shih, C.-D. Chen, W.-C. Lai, C.R.C. Wang. The shape transition of gold nanorods. *Langmuir* **15**, 701 (1999).
24. C.J. Murphy, T.K. Sau, A.M. Gole, C.J. Orendorff, J. Gao, L. Gou, S.E. Hunyadi, T. Li. Anisotropic metal nanoparticles: synthesis, assembly, and optical applications. *J. Phys. Chem. B* **109**, 13857 (2005).
25. X. Xu, M.B. Cortie. Shape change and color gamut in gold nanorods, dumbbells, and dog bones. *Adv. Funct. Mater.* **16**, 2170 (2006).
26. B. Saute, R. Narayanan. Solution-based direct readout surface enhanced Raman spectroscopic (SERS) detection of ultra-low levels of thiram with dogbone shaped gold nanoparticles. *Analyst* **136**, 527 (2011).
27. H. Chen, L. Shao, Q. Li, J. Wang. Gold nanorods and their plasmonic properties. *Chem. Soc. Rev.* **42**, 2679 (2013).
28. M. Grzelczak, A. Sánchez-Iglesias, B. Rodríguez-González, R. Alvarez-Puebla, J. Pérez-Juste, L.M. Liz-Marzán. Influence of iodide ions on the growth of gold nanorods: Tuning tip curvature and surface plasmon resonance. *Adv. Funct. Mater.* **18**, 3780 (2008).
29. P. Wang, M. Liu, G. Gao, S. Zhang, H. Shi, Z. Li, L. Zhang, Y. Fang. From gold nanorods to nanodumbbells: a different way to tailor surface plasmon resonances by a chemical route. *J. Mater. Chem.* **22**, 24006 (2012).
30. D.A. Zweifel, A. Wei. Sulfide-arrested growth of gold nanorods. *Chem. Mater.* **17**, 4256 (2005).
31. E. Carbó-Argibay, B. Rodríguez-González, S. Gómez-Graña, A. Guerrero-Martinez, I. Pastoriza-Santos, J. Pérez-Juste, L.M. Liz-Marzán. The crystalline structure of gold nanorods revisited: Evidence for higher-index lateral facets. *Angew. Chem. Int. Ed.* **49**, 9397 (2010).
32. H. Katz-Boon, C.J. Rossouw, M. Weyland, A.M. Funston, P. Mulvaney, J. Etheridge. Three-dimensional morphology and crystallography of gold nanorods. *Nano Lett.* **11**, 273 (2011).

33. B. Rodríguez-González, F. Attouchi, M.F. Cardinal, V. Myroshnychenko, O. Stéphan, F.J. Garcia de Abajo, L.M. Liz-Marzán, M. Kociak. Surface plasmon mapping of dumbbell-shaped gold nanorods: The effect of silver coating. *Langmuir* **28**, 9063 (2012).
34. M. Grzelczak, A. Sánchez-Iglesias, H.H. Mezerji, S. Bals, J. Pérez-Juste, L.M. Liz-Marzán. Steric hindrance induces crosslike self-assembly of gold nanodumbbells. *Nano Lett.* **12**, 4380 (2012).
35. M.F. Cardinal, B. Rodríguez-González, R.A. Alvarez-Puebla, J. Pérez-Juste, L.M. Liz-Marzán. Modulation of localized surface plasmons and sers response in gold dumbbells through silver coating. *J. Phys. Chem. C* **114**, 10417 (2010).
36. D. Constantin. Why the aspect ratio? Shape equivalence for the extinction spectra of gold nanoparticles. *Eur. Phys. J. E.* **38**, 116 (2015).
37. N.L. Dmitruk, A.V. Goncharenko, E.F. Venger. *Optics of Small Particles and Composite Media* (Naukova Dumka, 2009) (in Ukrainian) [ISBN: 978-966-00-0948-8].

Received 31.05.25.
Translated from Ukrainian by O.I. Voitenko

А.В. Коротун

РЕЗОНАНСНІ ОПТИЧНІ ЯВИЩА В МЕТАЛЕВИХ ГАНТЕЛЕПОДІБНИХ НАНОЧАСТИНКАХ. ПІДХІД ЕКВІВАЛЕНТНОГО СФЕРОЇДА

В класичному наближенні одержано вирази для діагональних компонент тензора добротності, підсилення локальних електричних полів та поляризовності, а також перерізів поглинання, розсіювання та екстинкції для металевих гантелеподібних наночастинок. Для побудови аналітичної теорії використано підхід еквівалентного сфероїда. Наведено результати розрахунків вказаних оптичних характеристик для гантелеподібних наночастинок різних розмірів і різних матеріалів. Проаналізовано вплив зміни ефективного аспектного відношення на еволюцію частотних залежностей досліджуваних оптичних характеристик. Показано доцільність використання гантелеподібних наночастинок із малим аспектним відношенням в наномедицині та в оптичних високодобротних резонаторах із малим аспектним відношенням.

Ключові слова: гантелеподібна наночастинка, тензори поляризовності, підсилення полів, добротності, перерізи поглинання, розсіювання та екстинкції, підхід еквівалентного сфероїда, ефективне аспектне відношення, поверхневий плазмонний резонанс.